

Confronting Reward Overoptimization for Diffusion Models: A Perspective of Inductive and Primacy Biases

Ziyi Zhang¹ Sen Zhang² Yibing Zhan³ Yong Luo¹ Yonggang Wen⁴ Dacheng Tao⁴

Abstract

Bridging the gap between diffusion models and human preferences is crucial for their integration into practical generative workflows. While optimizing downstream reward models has emerged as a promising alignment strategy, concerns arise regarding the risk of excessive optimization with learned reward models, which potentially compromises ground-truth performance. In this work, we confront the reward overoptimization problem in diffusion model alignment through the lenses of both inductive and primacy biases. We first identify the divergence of current methods from the temporal inductive bias inherent in the multi-step denoising process of diffusion models as a potential source of overoptimization. Then, we surprisingly discover that dormant neurons in our critic model act as a regularization against overoptimization, while active neurons reflect primacy bias in this setting. Motivated by these observations, we propose Temporal Diffusion Policy Optimization with critic active neuron Reset (TDPO-R), a policy gradient algorithm that exploits the temporal inductive bias of intermediate timesteps, along with a novel reset strategy that targets active neurons to counteract the primacy bias. Empirical results demonstrate the superior efficacy of our algorithms in mitigating reward overoptimization.

1. Introduction

Diffusion models (Sohl-Dickstein et al., 2015) represent the state-of-the-art in generative modeling for continuous data, particularly excelling in text-to-image generation (Rombach et al., 2022). Traditional training methodologies for diffu-

¹School of Computer Science, Wuhan University, China
²The University of Sydney, Australia ³JD Explore Academy, Beijing, China ⁴Nanyang Technological University, Singapore.
 Correspondence to: Ziyi Zhang <ziyizhang27@whu.edu.cn>, Sen Zhang <sen.zhang@sydney.edu.au>, Yibing Zhan <zybjy@mail.ustc.edu.cn>, Yong Luo <luoyong@whu.edu.cn>, Yonggang Wen <ygw@ntu.edu.sg>, Dacheng Tao <dacheng.tao@gmail.com>.

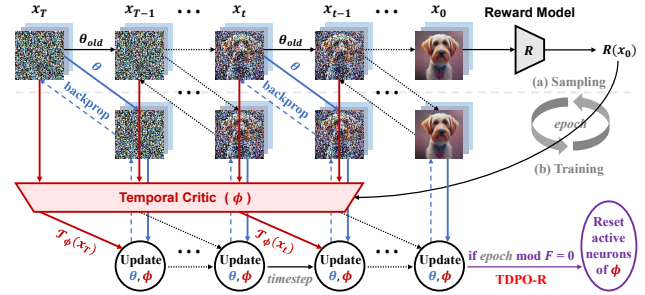


Figure 1. TDPO-R first samples trajectories $(x_T, x_{T-1}, \dots, x_0)$ from the denoising process of a fixed diffusion model parameterized by θ_{old} . For each denoising timestep t , it conducts a one-step denoising of the current diffusion model parameterized by θ , estimates a temporal reward $\hat{\mathcal{T}}_\phi(x_t)$ by a temporal critic parameterized by ϕ , and updates the gradients for both θ and ϕ according to the corresponding temporal reward. Additionally, TDPO-R resets active neurons of ϕ at the end of every F epochs.

sion models predominantly adhere to a maximum likelihood objective. However, such approaches may not inherently prioritize the optimization of downstream objectives, such as image aesthetic quality (Schuhmann et al., 2022) or human preferences (Xu et al., 2023; Wu et al., 2023a). To align pre-trained diffusion models with downstream objectives, researchers have explored using learned or handcrafted reward functions to finetune these models. Typical solutions along this research direction can be categorized into supervised learning (Lee et al., 2023; Wu et al., 2023b; Dong et al., 2023), reinforcement learning (RL) (Fan et al., 2023; Black et al., 2024), and backpropagation through sampling (Clark et al., 2024; Prabhudesai et al., 2023).

Despite the promise of reward-driven approaches, reward overoptimization remains a fundamental and under-researched challenge. This phenomenon, characterized by overfitting learned or handcrafted reward models, stems from the inherent limitations of these models in capturing the full spectrum of human intent. In image generation, reward overoptimization typically manifests as fidelity deterioration or continual degradation in cross-reward generalization against out-of-domain reward functions. Additionally, sample efficiency further complicates this issue. Notably, while RL-based methods (Fan et al., 2023; Black

et al., 2024) exhibit relatively lower susceptibility to reward overoptimization, this advantage comes at the expense of diminished sample efficiency due to the extra sampling process isolated from training. This further entails a trade-off between sample efficiency and reward overoptimization.

Regrettably, the underlying causes of reward overoptimization in diffusion model alignment remain unclear, which is the primary concern of this work. To this end, we systematically investigate this problem from the perspective of both inductive and primacy biases. Firstly, within the context of deep RL, the congruence between the inductive biases of the problem and the corresponding algorithm plays a crucial role in achieving robust generalization (Zhang et al., 2018). However, current reward-driven alignment approaches exclusively optimize rewards computed from the final generated images while overlooking the information in intermediate timesteps. This inherently introduces a divergence from the temporal inductive bias corresponding to the multi-step denoising process of diffusion models. Consequently, the model prioritizes features associated with late-stage denoising timesteps, leading to overfitting and misalignment between the desired reward and the true quality of the generation process.

Secondly, primacy bias (Nikishin et al., 2022), the tendency of deep RL agents to overfit early training experiences, poses another potential source of reward overoptimization. To this end, we investigate the neuron states as internal indicators of primacy bias. Although Sokar et al. (2023) suggest that dormant neurons in deep RL agents have a negative effect on the model capacity and resetting dormant neurons reduces this effect, we surprisingly discover that dormant neurons instead act as an adaptive regularization against reward overoptimization, while active neurons appear to be susceptible to the primacy bias towards this phenomenon.

Motivated by the above observations, we propose Temporal Diffusion Policy Optimization with critic active neuron Reset (TDPO-R), a novel policy gradient algorithm that exploits the temporal inductive bias of intermediate timesteps and mitigates the primacy bias stemming from active neurons. Specifically, TDPO-R assigns each intermediate timestep a temporal reward which is derived by learning a temporal critic function. The diffusion model and the temporal critic are then optimized simultaneously via gradient descent with per-timestep updates. Accordingly, the alignment between the temporal rewards and the per-timestep gradient updates not only mitigates reward overoptimization, but also improves sample efficiency by balancing the update frequency and the optimization stability. To counteract the primacy bias, we present a periodic reset strategy for active neurons rather than dormant ones, which further alleviates the reward overoptimization problem.

We deploy the proposed TDPO-R with Stable Diffusion

v1.4 (Rombach et al., 2022) and conduct empirical evaluations using multiple reward functions over a variety of prompt sets. We first employ individual reward functions to quantitatively measure the sample efficiency and model performance per task. Then we introduce a novel metric of cross-reward generalization as a proxy for the quantitative evaluation of reward overoptimization. Evaluation results demonstrate the superior performance of our algorithms in the trade-off between sample efficiency and cross-reward generalization compared to state-of-the-art methods. In addition, we validate that our active neuron reset strategy significantly contributes to the further mitigation of reward overoptimization in TDPO, as evidenced by the outstanding performance in cross-reward generalization, as well as the fidelity and diversity observed in high-reward qualitative results. The main contributions of this paper are as follows:

- To the best of our knowledge, this is the first work that investigates the underlying causes of reward overoptimization in diffusion model alignment from the perspective of inductive and primacy biases.
- We identify the temporal inductive bias in the diffusion model and exploit it by the proposed TDPO-R that includes temporal alignment and per-timestep update, which not only mitigates reward overoptimization but also improves sample efficiency.
- We surprisingly discover that dormant neurons act as an adaptive regularization against reward overoptimization, and present a periodic reset strategy of active neurons to overcome this primacy bias, further alleviating the reward overoptimization problem.
- We develop a quantitative metric of cross-reward generalization as a proxy for the evaluation of reward overoptimization, and demonstrate the superior efficacy of our methods in trading off efficiency and generalization.

2. Related Work

Reward finetuning of diffusion models. Lee et al. (2023) and Wu et al. (2023b) finetune diffusion models on rewards using supervised learning. Dong et al. (2023) present an online variant of these supervised learning-based methods. Fan et al. (2023) and Black et al. (2024) explore using policy gradient-based RL algorithms to align diffusion models with arbitrary rewards. Clark et al. (2024) and Prabhudesai et al. (2023) finetune diffusion models by backpropagating gradients of differentiable reward functions and truncate backpropagation to a few sampling steps. All these works use timestep-independent rewards based on fully-generated images, precluding intermediate samples in the denoising process. In contrast, we introduce timestep-dependent rewards for intermediate samples, and optimize diffusion models on

these rewards at temporal granularity. More importantly, none of these works explicitly address reward overoptimization, which is the main focus of our work.

Reward hacking and overoptimization. Reward overoptimization (Gao et al., 2023; Moskovitz et al., 2024), also termed “reward hacking”, refers to the detrimental phenomenon where optimizing too much on imperfect reward functions hinders the model performance on the true objectives. To address this issue, two widely employed strategies are early stopping (Black et al., 2024) and Kullback-Leibler (KL) regularization (Fan et al., 2023). However, there still exists a lack of statistical evidence and understanding of their efficacy in reducing overoptimization. In this work, we investigate the underlying causes of reward overoptimization from the perspective of inductive and primacy biases. In addition, we are the first to design large-scale quantitative evaluations based on the cross-reward generalization metric for reward overoptimization in diffusion model alignment.

Primacy bias and plasticity loss. Primacy bias (Nikishin et al., 2022) is also identified by a variety of other terminologies, including implicit under-parameterization (Kumar et al., 2020), capacity loss (Lyle et al., 2021), and dormant neuron phenomenon (Sokar et al., 2023). All of these can be generalized as plasticity loss (Lyle et al., 2023; Ma et al., 2024), i.e., loss of ability to learn and generalize. Resetting the last layer of an agent network (Nikishin et al., 2022) retrieves plasticity, but may cause knowledge forgetting. Sokar et al. (2023) suggest that dormant neurons in agent networks have a negative effect on model plasticity, which can be mitigated by resetting these neurons. However, our empirical findings present a surprising deviation from this conclusion within the context of reward overoptimization, which unveils that dormant neurons act as a regularization that benefits our model, offering a new perspective for understanding neuron states and overcoming primacy bias.

3. Preliminaries

3.1. Denoising Diffusion Probabilistic Models

This work is built upon Denoising Diffusion Probabilistic Models (DDPM) (Ho et al., 2020), a well-established diffusion backbone that learns to model a probability distribution $p(x_0)$ by reversing a Markovian forward process $q(x_t|x_{t-1})$ that iteratively adds Gaussian noise towards the desired sample x_0 at each diffusion timestep t . The reverse process is modeled by a denoising neural network $\mu_\theta(x_t, t)$ to predict its posterior mean $\tilde{\mu}(x_0, x_t)$, which is a weighted average of x_0 and x_t . The network is parameterized by θ and trained using the following objective:

$$\mathbb{E}_{x_0 \sim p(x_0), t \sim [1, T], x_t \sim q(x_t|x_0)} [\|\tilde{\mu}(x_0, x_t) - \mu_\theta(x_t, t)\|^2]. \quad (1)$$

Additionally, DDPM is readily extended to the conditional

generative modeling of $p(x_0|c)$, where c is a conditional signal, such as a text prompt, processed by a conditional denoising network $\mu_\theta(x_t, t, c)$. To sample from a learned denoising process $p_\theta(x_{t-1}|x_t, c)$, one begins by drawing a Gaussian noisy sample $x_T \sim \mathcal{N}(0, I)$, and then employs a specific sampling scheduler (Ho et al., 2020; Song et al., 2021), which iteratively generates subsequent samples x_{T-1}, \dots, x_0 according to outputs from the denoising network μ_θ . An intermediate timestep of the denoising process with the noise variance σ_t^2 can be written as:

$$p_\theta(x_{t-1}|x_t, c) = \mathcal{N}(x_{t-1}; \mu_\theta(x_t, t, c), \sigma_t^2 I). \quad (2)$$

3.2. Reinforcement Learning

Markov Decision Process (MDP). MDP provides a mathematical framework for modeling decision-making problems. We consider finite MDP in this work, where the agent acts iteratively at each of a sequence of discrete timesteps $t \in (0, 1, 2, \dots)$, up to a maximum timestep T . At each timestep t , the agent perceives a state $s_t \in \mathcal{S}$, and selects an action $a_t \in \mathcal{A}$ by a policy $\pi(a_t|s_t)$, where \mathcal{S}, \mathcal{A} are state and action spaces respectively. One timestep later, the agent receives a numerical reward $r(s_t, a_t)$ as a consequence of its action, and finds itself in a new state $s_{t+1} \sim P(s_{t+1}|s_t, a_t)$, where P denotes the transition probability function.

RL objective. Within the MDP framework, the interaction between the agent and the environment give rise to trajectories $\tau = (s_0, a_0, s_1, a_1, \dots, s_T, a_T)$, where each element represents a state-action pair at a specific timestep. Then the RL objective under this formulation is to find the policy that maximizes the expected accumulation of trajectory rewards:

$$\max_{\pi} \mathbb{E}_{\tau \sim p(\tau|\pi)} \left[\sum_{t=0}^T r(s_t, a_t) \right]. \quad (3)$$

4. Method

Now we delve into our approach to addressing the reward overoptimization problem in diffusion model alignment, focusing on the exploration of both inductive and primacy biases. Subsequently, we will introduce Temporal Diffusion Policy Optimization with critic active neuron Reset (TDPO-R), a policy gradient algorithm illustrated in Figure 1, which exploits the temporal inductive bias of intermediate denoising timesteps and incorporates a novel reset strategy that targets active neurons to counteract the primacy bias.

4.1. Temporal Diffusion Policy Optimization

In this section, we first revisit the multi-step MDP formulation of the denoising process in diffusion models, and identify a divergence of current alignment methods from the temporal inductive bias inherent in the denoising process.

We then reformulate this process by introducing intermediate rewards for each timestep, and provide an efficient approach to approximate these temporal rewards. Under this MDP formulation, we develop Temporal Diffusion Policy Optimization (TDPO), a policy gradient algorithm that performs a timestep-aware optimization of the denoising process via gradient descent with per-timestep updates, to exploit the temporal inductive bias of intermediate timesteps and prevent overfitting to the reward of the final image.

Temporal inductive bias. To perform RL-based diffusion model alignment, Fan et al. (2023) and Black et al. (2024) map the denoising process in diffusion models to a multi-step MDP, in which the trajectories $(x_T, x_{T-1}, \dots, x_0)$ correspond to the intermediate images sampled during the denoising process. In their settings, the cumulative rewards for all trajectories are condensed into a singular value $R(x_0, c)$, which is exclusively computed on the final sample x_0 , precluding the noisy samples x_t obtained at each intermediate timestep t . This timestep-independent reward definition diverges from the temporal inductive bias inherent in the intermediate timesteps of the multi-step denoising process, thereby posing a potential risk of overfitting to $R(x_0, c)$.

Denoising as MDP with temporal rewards. To inherit and exploit the temporal inductive bias within the denoising process, we characterize this process as a multi-step MDP with timestep-dependent trajectory rewards $\mathcal{T}(x_t, c)$:

$$\begin{aligned} s_t &\triangleq (x_{T-t}, t, c), & \rho_0(s_0) &\triangleq (p(c), \delta_0, \mathcal{N}(0, I)), \\ a_t &\triangleq x_{T-t-1}, & P(s_{t+1}|s_t, a_t) &\triangleq (\delta_c, \delta_{t+1}, \delta_{x_{T-t-1}}), \\ r(s_t, a_t) &\triangleq \mathcal{T}(x_{T-t-1}, c), & \pi(a_t|s_t) &\triangleq p_\theta(x_{T-t-1}|x_{T-t}, c), \end{aligned} \quad (4)$$

where ρ_0 is the initial state distribution, δ_z is the Dirac delta distribution at z , and optimizing the policy π is equivalent to finetuning the diffusion model parameterized by θ . This formulation diverges from the ones presented in (Fan et al., 2023; Black et al., 2024), in terms of the timestep-dependent definition of trajectory rewards. We refer $\mathcal{T}(x_t, c)$ to the intermediate reward w.r.t. the noisy image x_t at each timestep t of the denoising process.

Accordingly, this formulation informs a timestep-aware optimization of the denoising process $p_\theta(x_{0:T}|c)$, which exploits the aforementioned temporal inductive bias. This optimization procedure is driven by the objective of maximizing the expected temporal rewards at each denoising timestep, i.e.,

$$\max_{\theta} \mathbb{E}_{p(c)} \mathbb{E}_{p_\theta(x_{0:T}|c)} [\mathcal{T}(x_t, c)]. \quad (5)$$

Temporal reward approximation. Prevalent reward models such as aesthetic predictor (Schuhmann et al., 2022) and ImageReward (Xu et al., 2023) are usually trained on the distributions of the final clean images rather than intermediate noisy samples within the denoising process. Consequently, it is not feasible to derive the temporal rewards directly from

these reward models. An intuitive solution for this problem involves retraining reward models on noisy images, but it restricts the direct utilization of off-the-shelf reward models and imposes excessive additional training overhead.

To address this issue, we present an efficient approach in this section. In particular, we first utilize off-the-shelf reward models to compute the reward function for each final clean image x_0 , denoted as $R(x_0, c)$. Then we approximate the temporal reward $\mathcal{T}(x_t, c)$ for each intermediate noisy image x_t by learning a temporal critic function $\mathcal{T}_\phi(x_t, c)$ parameterized by ϕ . To facilitate the learning process, we further use $R(x_0, c)$ as an anchor and compute $\mathcal{T}_\phi(x_t, c)$ as:

$$\mathcal{T}(x_t, c) \triangleq \mathbb{E}[\mathcal{T}_\phi(x_t, c)] \triangleq \mathbb{E}[R(x_0, c) - \mathcal{R}_\phi(x_t, c)], \quad (6)$$

where $\mathcal{R}_\phi(x_t, c)$ is the prediction function of a temporal residual for each temporal reward, which is trained in conjunction with the policy over all denoising timesteps.

Nonetheless, learning $\mathcal{R}_\phi(x_t, c)$ presents a non-trivial challenge, since we need to evaluate temporal rewards at each timestep. A naive implementation of the temporal critic with a comparable number of training parameters as the reward model can incur significant training complexity. To address this challenge, we leverage the encoders of target reward models to extract embeddings from each intermediate image of the denoising process. These embeddings serve as the input to a lightweight Multi-Layer Perceptron (MLP) with only 5 layers, acting as our $\mathcal{R}_\phi(x_t, c)$ function:

$$\mathcal{R}_\phi(x_t, c) = \text{MLP}_\phi(\text{Encoder}_R(x_t, c)). \quad (7)$$

Encoder alignment. This practice of reusing encoders establishes an alignment between the encoders of both the reward model and the temporal critic. This alignment tends to be critical for overall performance, as it ensures consistency in feature representations and enables the temporal critic to inherit the inductive bias of the reward model during initial training. This inductive bias is further dynamically refined during subsequent training, adapting to the evolving intermediate states encountered during the denoising process. Beyond performance gains, encoder alignment also offers a compelling advantage in memory efficiency, as the need to store a separate encoder for the temporal critic is eliminated. Implementation details and extended analysis of encoder alignment are provided in Appendix E.

Temporal gradient estimation. Given the temporal rewards in Eq. (6) and (7), we can estimate the gradient of the objective in Eq. (5) w.r.t. the policy parameters θ at temporal granularity. We first sample trajectories $(x_T, x_{T-1}, \dots, x_0)$ from the denoising process $p_\theta(x_{0:T}|c)$, and collect the likelihood gradients with respect to θ , i.e., $\nabla_\theta p_\theta(x_{t-1}|x_t, c)$. To reuse the trajectories sampled by an old policy parameterized by θ_{old} , we employ importance sampling (Kakade

& Langford, 2002), which reweights the temporal rewards by the corresponding probability ratio. Then the temporal gradient at each denoising timestep reads:

$$\mathbb{E}_{p(c)} \mathbb{E}_{p_\theta(x_{0:t}|c)} \left[-\mathcal{T}_\phi(x_t, c) \nabla_\theta \frac{p_\theta(x_{t-1}|x_t, c)}{p_{\theta_{\text{old}}}(x_{t-1}|x_t, c)} \right]. \quad (8)$$

Furthermore, we apply an regularization objective to control the potential variance of temporal reward estimation:

$$\mathbb{E}_{p(c)} \mathbb{E}_{p_\theta(x_{0:t}|c)} \left[\left(\hat{\mathcal{R}}_\phi(x_t, c) - R(x_0, c) \right)^2 \right]. \quad (9)$$

Per-timestep gradient update. We concurrently update the policy parameters θ and the critic parameters ϕ via gradient descent. In particular, we perform each update in a per-timestep manner, in contrast to other methods that employ per-batch updates, emphasizing the temporal granularity of our approach. A per-timestep gradient update for θ or ϕ is performed via the averaged batch gradient below:

$$\frac{1}{B} \sum_{i=1}^B \mathbb{E}_{p(c_i) p_\theta(x_{0:t}^i | c_i)} \left[\nabla_\alpha G_\alpha(x_t^i, c_i) \right], \alpha \in \{\theta, \phi\}, \quad (10)$$

where B is the batch size, and $\nabla_\alpha G_\alpha(x_t^i, c_i)$ is the objective gradient estimate with respect to θ or ϕ at each timestep t in each mini-batch i . The motivation and advantages of this per-timestep update strategy are described as follows:

Remark on per-timestep update. In most cases of deep RL, a higher gradient update frequency often results in faster convergence but worse stability. In our settings, we operate on samples spanning two dimensions: timesteps and mini-batches, allowing us to elevate the gradient update frequency by reducing the sizes of these dimensions. However, reducing the dimension sizes introduces lower variance in sample distributions, potentially leading to overfitting. Intuitively, the variance of sample distributions within a per-timestep context (encompassing all mini-batches) exceeds that within a per-minibatch context (covering all timesteps derived from a shared Gaussian distribution). This suggests that reducing the number of timesteps per update represents a relatively secure approach for expediting convergence, while it still poses a risk of overfitting to the timestep-independent reward exclusively based on the final image. To mitigate this risk, we incorporate the temporal rewards as fine-grained guidance for the per-timestep updates, thereby improving sample efficiency while ensuring overall stability.

4.2. Primacy Bias in Diffusion Policy Optimization

In Section 4.1, we presented TDPO to incorporate temporal inductive bias and relieve reward overoptimization. Additionally, primacy bias presents another critical source of this phenomenon, which could be exacerbated by the limited

Algorithm 1 TDPO-R: Temporal diffusion policy optimization (with critic active neuron reset)

Input: Diffusion model parameters θ , critic model parameters ϕ , context distribution $p(c)$, epochs E , timesteps T , batch size B , and neuron reset frequency F

for $e = 1, \dots, E$ **do**

Obtain samples $\{c_i \sim p(c), x_{0:T}^i \sim p_\theta(x_{0:T}|c_i)\}_{i=1}^B$

Compute temporal rewards according to Eq. (6)

for $t = T, \dots, 1$ **do**

Update θ, ϕ at timestep t according to Eq. (10)

end for

if $e \bmod F == 0$ **then**

Obtain neuron masks for ϕ according to Eq. (12)

Reinitialize ϕ where the neuron mask is *true*

end if

end for

model capacity of our temporal critic. In this section, we investigate how the states of neurons in our model reflect such primacy bias and the corresponding effect on reward overoptimization when aligning diffusion models.

Neuron activations and states. Following Sokar et al. (2023), we use neuron activation in deep neural networks to categorize the states of neurons. We first consider each feature map between two layers within a network module as the state of a neuron. For an input x of distribution \mathcal{D} , we denote the activation of a neuron n in a module m as $a_n^m(x)$, and compute an activation score \mathcal{A}_n^m for each neuron n in the module m as:

$$\mathcal{A}_n^m = \frac{\mathbb{E}_{x \in \mathcal{D}} |a_n^m(x)|}{\frac{1}{N^m} \sum_{n \in N^m} \mathbb{E}_{x \in \mathcal{D}} |a_n^m(x)|}, \quad (11)$$

where N^m is the number of neurons in the module m , and the expected activation over \mathcal{D} is normalized by the average of all activations. Then we set a threshold for this activation score to categorize all neurons in our models into two opposite states. If the activation score of a neuron is above the threshold, we say the neuron is active, otherwise it is regarded as dormant.

Dormant neurons are indispensable. Accordingly, we conduct empirical evaluations to investigate the effects of different neuron states on reward overoptimization during the training process of TDPO. We detect the percentage of dormant neurons in our critic model, and observe a slow ascent of this percentage during training. To directly influence the neuron states during training, we periodically reset neurons of a given state by reinitializing its parameters to the original distributions. Surprisingly, we find that while resetting dormant neurons periodically reduces the dormant percentage at all training steps, it actually exacerbates reward overoptimization. This deviates from the conclusion in (Sokar et al., 2023) where dormant neurons in deep RL

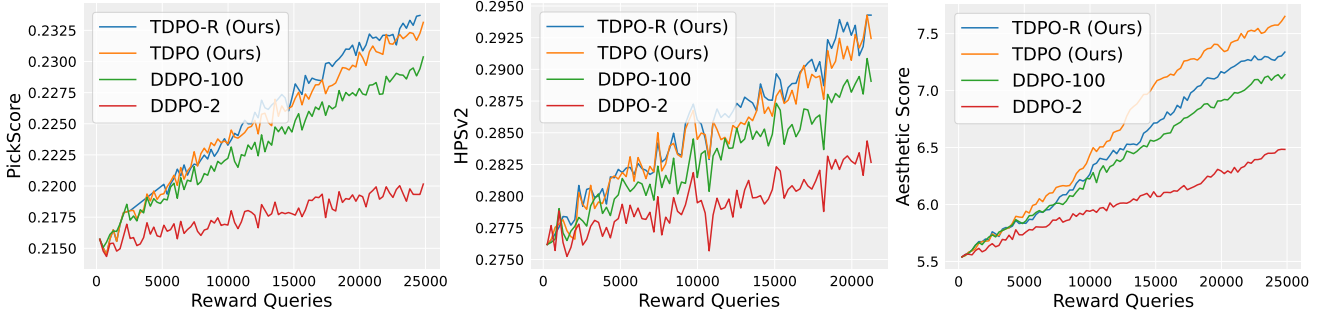


Figure 2. Quantitative evaluation results for the efficacy of our TDPO and TDPO-R in improving sample efficiency when finetuning diffusion models on the reward functions of PickScore (left), HPSv2 (middle), and Aesthetic Score (right), compared to DDPO with the update frequencies of 2 (DDPO-2) and 100 (DDPO-100) per epoch.

were found to hinder model capacity and necessitate resets.

Active neurons reflect primacy bias. We further explore resetting active neurons in the critic. Although this does not reduce the dormant percentage, it effectively mitigates reward overoptimization. Interestingly, resetting all neurons in the critic also exacerbates reward overoptimization, albeit to a lesser degree compared to solely resetting dormant neurons. We posit that dormant neurons in the critic model act as an adaptive regularization mechanism against overoptimization to imperfect rewards, which suggests resetting dormant neurons may damage this implicit regularization. Our findings imply that, within the context of reward overoptimization, primacy bias manifests primarily in active neurons. Consequently, periodically resetting these neurons offers a potential mitigation strategy, encouraging the model to learn new regularization patterns without forgetting crucial past regularization. Further details and analyses supporting this observation are provided in Section 5.3 and Appendix B.

We further analyze the effect of the neuron states in the policy model. Since we adopt Low-Rank Adaptation (LoRA) (Hu et al., 2022) for the policy, only neurons within the LoRA layers can be reset. We detect very few dormant neurons, and resetting them makes no significant difference to the results. In this case, resetting active neurons causes catastrophic forgetting and heavily hinders learning.

TDPO with critic active neuron Reset (TDPO-R). Motivated by the above analyses, we present TDPO-R, a variant of TDPO that periodically resets the active neurons in the critic model with a frequency F . In practice, to reinitialize the model parameters ϕ_a corresponding to the active neurons, we compute a neuron mask for each module m :

$$\text{Mask}^m = [\mathcal{A}_n^m > 0]_{n=1}^{N^m}, \tag{12}$$

where each boolean value in it is set to true if the corresponding activation score $\mathcal{A}_n^m > 0$. This neuron mask is used to reinitialize the weights of both the incoming and outgo-

ing layers corresponding to the active neurons in module m . The pseudo-code of TDPO-R is summarized in Algorithm 1.

In neuroscience, there are several studies (Rotheneichner et al., 2018; Ovsepian, 2019; Benedetti & Couillard-Despres, 2022) investigating the function of dormant neurons. According to Ovsepian (2019), most neurons in the brain do not fire action potentials and remain dormant for a long time. These dormant neurons are formed during evolution, but are far from the scope of natural selection as they avoid regular functional tasks. However, under the influence of stress and disease, they occasionally become active, which can lead to various neurological and psychological disease symptoms and behavioral abnormalities. Interestingly, this conclusion mirrors our observation that resetting dormant neurons could be harmful for mitigating reward overoptimization.

5. Empirical Evaluations

We conduct comprehensive experiments to validate the efficacy of our algorithms on both sample efficiency and reward overoptimization alleviation when aligning text-to-image diffusion models with diverse reward functions.

5.1. Implementation Details

Baselines. We compare our algorithms with state-of-the-art baselines¹, including pre-trained Stable Diffusion (Rom-bach et al., 2022), Denoising Diffusion Policy Optimization (DDPO) (Black et al., 2024), and AlignProp (Prabhudesai et al., 2023). We use the official PyTorch codebase of DDPO for result reproduction. Following DDPO, we use Stable Diffusion v1.4 as the base generative model. For a fair comparison, we reproduce AlignProp using Stable Diffusion v1.4, while their reported results are based on v1.5.

¹Additional baselines, including DRaFT (Clark et al., 2024) that lacks open-source code, and DPOK (Fan et al., 2023) and ReFL (Xu et al., 2023) that underperform DDPO and AlignProp, are omitted in our reproductions due to the resource constraints.

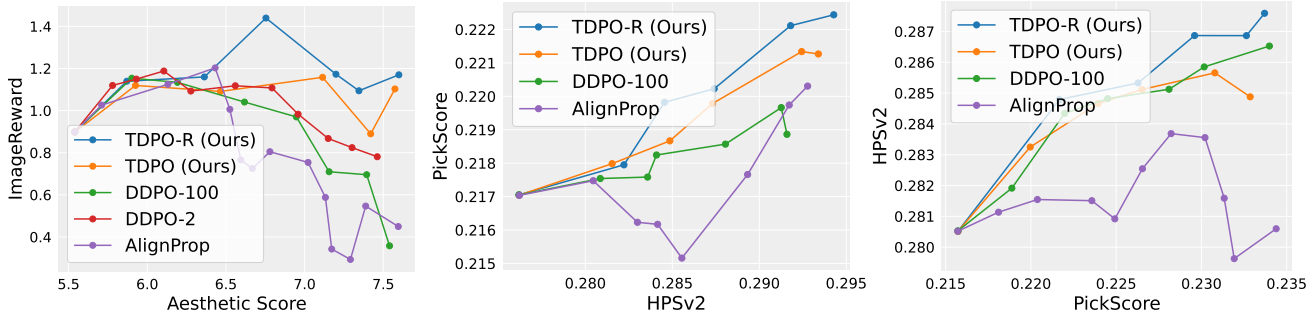


Figure 3. Out-of-domain evaluation results via cross-reward generalization against ImageReward (left), PickScore (middle), and HPSv2 (right) when finetuning diffusion models on Aesthetic Score (left), HPSv2 (middle), and PickScore (right), respectively.

Reward functions. To demonstrate the generalizability of our method, we perform training and evaluation on diverse reward functions, in which (a) **Aesthetic Score** is implemented using the LAION aesthetic predictor (Schuhmann et al., 2022) and a text prompt set of 45 animal names as in (Black et al., 2024); (b) **PickScore** (Kirstain et al., 2023) is employed for human preference finetuning, where we use the same prompt set as for Aesthetic Score; (c) **Human Preference Score v2** (HPSv2) (Wu et al., 2023a) presents an alternative reward function for human preference finetuning, along with 802 prompts drawn from Human Preference Dataset v2, and (d) **ImageReward** (Xu et al., 2023) is employed for the evaluation of cross-reward generalization.

To establish a consistent benchmark, the training procedures and configurations of our algorithms are based on the official PyTorch implementation of DDPO, which adopts LoRA (Hu et al., 2022) to reduce memory and computation cost.

5.2. Sample Efficiency in Diffusion Model Alignment

We employ TDPO and TDPO-R to separately finetune Stable Diffusion v1.4 on Aesthetic Score, PickScore, and HPSv2. We report the average reward over samples at each training interval w.r.t. specific number of reward queries, as the indicator of sample efficiency. TDPO(-R) performs each gradient update in a per-timestep manner with all batch samples averaged, resulting in a higher update frequency (100 gradient updates per epoch) compared to the original DDPO implementation (2 gradient updates per epoch). Thus, for a direct comparison, we further reproduce DDPO using the same update frequency as ours. Figure 2 shows that our algorithms consistently outperform both implementations of DDPO on each of the three rewards, demonstrating their effectiveness in improving sample efficiency. Notably, the high-frequency updates also accelerate training for DDPO, albeit at the cost of exacerbating reward overoptimization, as highlighted in Figure 3 and further discussed in Section 5.3.

5.3. Reward Overoptimization and Generalization

Cross-reward generalization. To quantitatively assess reward overoptimization, we introduce cross-reward generalization, where a model finetuned on one reward function is evaluated against another out-of-domain reward function. In Figure 3, TDPO and TDPO-R exhibit superior performance in three sets of cross-reward generalization evaluation with different reward functions, compared to DDPO and AlignProp, demonstrating the generalization ability of our methods to out-of-domain rewards.

Generalization to unseen prompts. In Figure 4, we show that the generalization abilities of TDPO and TDPO-R extend to out-of-domain text prompts that are not seen by the models during the finetuning process, which further demonstrates their robust capabilities in mitigating reward overoptimization. Implementation details and more evaluation results of unseen prompts are provided in Appendix C.

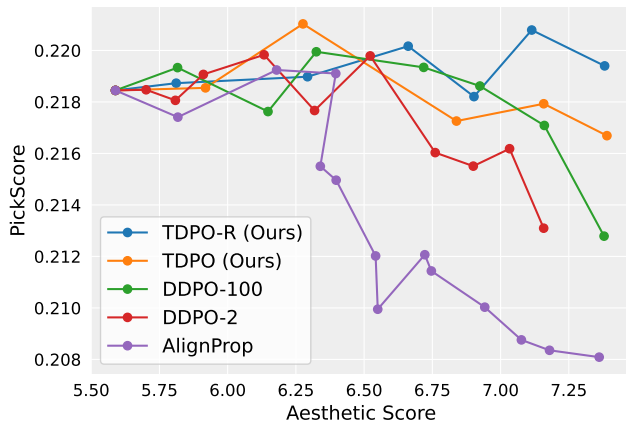


Figure 4. Cross-reward generalization results evaluated on a text prompt set of unseen animals when finetuning on Aesthetic Score.

Effects of neuron states. As mentioned in Section 4.2, we investigate the effects of neuron states on reward overoptimization by comparing TDPO-R and its variants with dif-



Figure 5. Image generation results sampled from models that are exclusively pre-trained or further finetuned on Aesthetic Score via AlignProp, DDPO-2, DDPO-100, as well as our TDPO and TDPO-R. For a fair comparison, all images are generated using a fixed random seed of 42, and those from the fine-tuned models achieve the same degree of rewards at around 7 ± 0.1 .

ferent reset strategies. In Figure 6, we present the results of cross-reward generalization to ImageReward for the variants that reset all, dormant, and active neurons in our critic model with the activation score threshold set to 0. For the variant that resets dormant neurons in our policy model, we set the threshold to 0.1, as using a threshold of 0 shows negligible differences from the original TDPO. The results are consistent with the effects discussed in Section 4.2. Further analyses and evaluation results are provided in Appendix B.

Alternate strategies for overoptimization. Both DDPO and AlignProp apply early stopping to prevent overoptimization, but the reliance on interactive inspection hinders its scalability. Fan et al. (2023) conduct an analysis of KL regularization in diffusion model alignment, while the quantitative evaluation on reward overoptimization is lacking. We also report the cross-reward generalization results of using KL regularization in Figure 6, which indicates that our neuron reset strategy is more effective for mitigating reward overoptimization compared to KL regularization.

5.4. Qualitative Comparison

We present a visual comparison of high-reward image generation results for the alignment methods in Figure 5, to qualitatively evaluate reward overoptimization when optimizing rewards to the same degree. The results from AlignProp and DDPO show notable saturation in terms of style, background, and sunlight, while our generation results manifest greater diversity in these aspects and exhibit higher fidelity in the meantime, which demonstrates the capabilities of TDPO and TDPO-R in mitigating reward overoptimization. Additionally, we also provide image generation results for generalization to unseen text prompts in Appendix C.

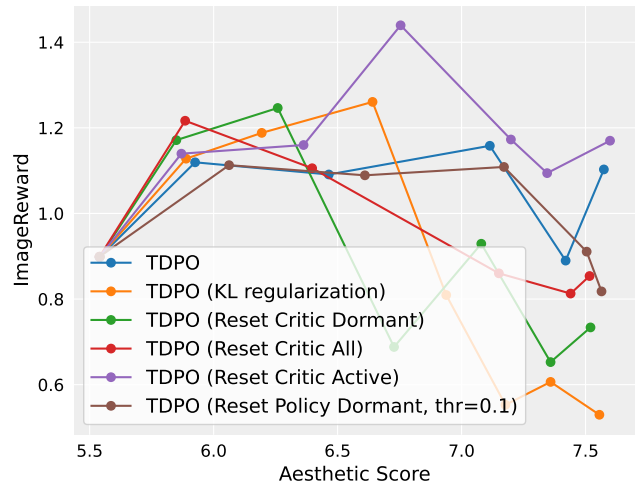


Figure 6. Evaluation results of cross-reward generalization to ImageReward when finetuning TDPO-R variants on Aesthetic Score.

6. Conclusion

In this work, we tackle the reward overoptimization problem in diffusion model alignment from the perspective of inductive and primacy biases. Specifically, we identify the temporal inductive bias inherent in diffusion models and make the surprising discovery that dormant neurons in our proposed temporal critic serve to mitigate reward overoptimization. Inspired by these findings, we present TDPO-R, which exploits the temporal inductive bias of intermediate denoising timesteps and optimizes diffusion models in alignment with them at temporal granularity. Empirical evaluations validate the effectiveness of the proposed method.

Limitations and future work. Constrained by computa-

tional resources, TDPO-R only operate on LoRA weights rather than all parameters of diffusion model, precluding a comprehensive analysis of the neuron states in this case. However, this work opens avenues for follow-up research on this problem. Furthermore, multi-reward learning in current research on diffusion models is still under-explored, highlighting a significant gap for future work. We hope that our work will also inspire future research on overoptimization in the context of multi-reward learning for diffusion models.

Impact Statements

This work contributes to the advancement of diffusion model alignment, with the potential to impact various aspects of society. Here, we highlight the key positive impacts:

Improved alignment of diffusion models. This work confronts the issue of reward overoptimization, which hinders the effective alignment of diffusion models with downstream applications. By mitigating this issue, we pave the way for the development of more reliable and trustworthy diffusion models that reflect human preferences, which empowers individuals and businesses to leverage the powerful capabilities of diffusion models for various creative applications.

Potential for broader applications. Beyond their direct impacts on diffusion models, the insights and techniques presented in this work, such as exploiting temporal inductive bias and addressing primacy bias through active neuron reset, may hold broader applicability in other domains of deep reinforcement learning, where similar challenges of overoptimization and bias hinder effective learning.

Furthermore, it is also essential to acknowledge potential societal concerns associated with this technology, such as:

Misuse of diffusion models. As diffusion models evolve towards enhanced alignment with human preferences and increased controllability, concerns regarding their potential misuse for malicious purposes, such as generating discriminatory or harmful contents, become increasingly salient. It is crucial to develop safeguards and ethical guidelines alongside technological advancements to mitigate these risks.

Unintended biases in reward learning. The effectiveness of diffusion model alignment relies on accurately capturing human preferences from reward models. However, human preferences can be subjective and biased. It's crucial to consider and mitigate potentially unintended biases in the data used to train the reward model to avoid exploiting and amplifying such biases in the generated outputs.

References

Bansal, A., Chu, H., Schwarzschild, A., Sengupta, S., Goldblum, M., Geiping, J., and Goldstein, T. Universal

guidance for diffusion models. In *Proceedings of the IEEE/CVF Conference on Computer Vision and Pattern Recognition*, pp. 843–852, 2023.

Beaumont, R., Wightman, R., Wang, P., Dayma, B., Wortsman, M., Blinkdl, Schuhmann, C., Jitsev, J., Ludwig, S., Cherti, M., and Mostaque, E. Large scale OpenCLIP: L/14, H/14 and G/14 trained on LAION-2B. *laion.ai*, 2022.

Benedetti, B. and Couillard-Despres, S. Why would the brain need dormant neuronal precursors? *Frontiers in Neuroscience*, 16, 2022.

Black, K., Janner, M., Du, Y., Kostrikov, I., and Levine, S. Training diffusion models with reinforcement learning. In *International Conference on Learning Representations*, 2024.

Clark, K., Vicol, P., Swersky, K., and Fleet, D. J. Directly fine-tuning diffusion models on differentiable rewards. In *International Conference on Learning Representations*, 2024.

Dhariwal, P. and Nichol, A. Q. Diffusion models beat GANs on image synthesis. *Advances in Neural Information Processing Systems*, 34:8780–8794, 2021.

Dong, H., Xiong, W., Goyal, D., Zhang, Y., Chow, W., Pan, R., Diao, S., Zhang, J., SHUM, K., and Zhang, T. RAFT: Reward ranked finetuning for generative foundation model alignment. *Transactions on Machine Learning Research*, 2023.

Fan, Y. and Lee, K. Optimizing DDPM sampling with shortcut fine-tuning. In *International Conference on Machine Learning*, pp. 9623–9639, 2023.

Fan, Y., Watkins, O., Du, Y., Liu, H., Ryu, M., Boutilier, C., Abbeel, P., Ghavamzadeh, M., Lee, K., and Lee, K. DPDK: Reinforcement learning for fine-tuning text-to-image diffusion models. *Advances in Neural Information Processing Systems*, 2023.

Gao, L., Schulman, J., and Hilton, J. Scaling laws for reward model overoptimization. In *International Conference on Machine Learning*, pp. 10835–10866, 2023.

Hao, Y., Chi, Z., Dong, L., and Wei, F. Optimizing prompts for text-to-image generation. *Advances in Neural Information Processing Systems*, 2023.

Ho, J. and Salimans, T. Classifier-free diffusion guidance. In *NeurIPS Workshop on Deep Generative Models and Downstream Applications*, 2021.

Ho, J., Jain, A., and Abbeel, P. Denoising diffusion probabilistic models. *Advances in Neural Information Processing Systems*, 33:6840–6851, 2020.

- Hu, E. J., Shen, Y., Wallis, P., Allen-Zhu, Z., Li, Y., Wang, S., Wang, L., and Chen, W. LoRA: Low-rank adaptation of large language models. In *International Conference on Learning Representations*, 2022.
- Kakade, S. and Langford, J. Approximately optimal approximate reinforcement learning. In *International Conference on Machine Learning*, pp. 267–274, 2002.
- Kirstain, Y., Polyak, A., Singer, U., Matiana, S., Penna, J., and Levy, O. Pick-a-pic: An open dataset of user preferences for text-to-image generation. *Advances in Neural Information Processing Systems*, 2023.
- Kumar, A., Agarwal, R., Ghosh, D., and Levine, S. Implicit under-parameterization inhibits data-efficient deep reinforcement learning. In *International Conference on Learning Representations*, 2020.
- Kumar, S., Marklund, H., and Roy, B. V. Maintaining plasticity via regenerative regularization. *arXiv preprint arXiv:2308.11958*, 2023.
- Lee, K., Liu, H., Ryu, M., Watkins, O., Du, Y., Boutilier, C., Abbeel, P., Ghavamzadeh, M., and Gu, S. S. Aligning text-to-image models using human feedback. *arXiv preprint arXiv:2302.12192*, 2023.
- Lyle, C., Rowland, M., and Dabney, W. Understanding and preventing capacity loss in reinforcement learning. In *International Conference on Learning Representations*, 2021.
- Lyle, C., Zheng, Z., Nikishin, E., Pires, B. Á., Pascanu, R., and Dabney, W. Understanding plasticity in neural networks. In *International Conference on Machine Learning*, pp. 23190–23211, 2023.
- Ma, G., Li, L., Zhang, S., Liu, Z., Wang, Z., Chen, Y., Shen, L., Wang, X., and Tao, D. Revisiting plasticity in visual reinforcement learning: Data, modules and training stages. In *International Conference on Learning Representations*, 2024.
- Maas, A. L., Hannun, A. Y., and Ng, A. Y. Rectifier nonlinearities improve neural network acoustic models. In *International Conference on Machine Learning*, 2013.
- Moskovitz, T., Singh, A. K., Strouse, D., Sandholm, T., Salakhutdinov, R., Dragan, A. D., and McAleer, S. Confronting reward model overoptimization with constrained RLHF. In *International Conference on Learning Representations*, 2024.
- Nikishin, E., Schwarzer, M., D’Oro, P., Bacon, P.-L., and Courville, A. The primacy bias in deep reinforcement learning. In *International Conference on Machine Learning*, pp. 16828–16847, 2022.
- Ovsepian, S. V. The dark matter of the brain. *Brain Structure and Function*, 224:973–983, 2019.
- Prabhudesai, M., Goyal, A., Pathak, D., and Fragkiadaki, K. Aligning text-to-image diffusion models with reward backpropagation. *arXiv preprint arXiv:2310.03739*, 2023.
- Radford, A., Kim, J. W., Hallacy, C., Ramesh, A., Goh, G., Agarwal, S., Sastry, G., Askell, A., Mishkin, P., Clark, J., Krueger, G., and Sutskever, I. Learning transferable visual models from natural language supervision. In *International Conference on Machine Learning*, pp. 8748–8763, 2021.
- Rombach, R., Blattmann, A., Lorenz, D., Esser, P., and Ommer, B. High-resolution image synthesis with latent diffusion models. In *Proceedings of the IEEE/CVF Conference on Computer Vision and Pattern Recognition*, pp. 10684–10695, 2022.
- Rotheneichner, P., Belles, M., Benedetti, B., König, R., Dannehl, D., Kreuzer, C., Zaunmair, P., Engelhardt, M., Aigner, L., Nacher, J., and Couillard-Despres, S. Cellular plasticity in the adult murine piriform cortex: Continuous maturation of dormant precursors into excitatory neurons. *Cerebral Cortex*, 28:2610–2621, 2018.
- Schuhmann, C., Beaumont, R., Vencu, R., Gordon, C. W., Wightman, R., Cherti, M., Coombes, T., Katta, A., Mullis, C., Wortsman, M., Schramowski, P., Kundurthy, S. R., Crowson, K., Schmidt, L., Kaczmarczyk, R., and Jitsev, J. LAION-5B: An open large-scale dataset for training next generation image-text models. *Advances in Neural Information Processing Systems*, 35:25278–25294, 2022.
- Schulman, J., Moritz, P., Levine, S., Jordan, M. I., and Abbeel, P. High-dimensional continuous control using generalized advantage estimation. In *International Conference on Learning Representations*, 2016.
- Sohl-Dickstein, J., Weiss, E., Maheswaranathan, N., and Ganguli, S. Deep unsupervised learning using nonequilibrium thermodynamics. In *International Conference on Machine Learning*, pp. 2256–2265, 2015.
- Sokar, G., Agarwal, R., Castro, P. S., and Evci, U. The dormant neuron phenomenon in deep reinforcement learning. In *International Conference on Machine Learning*, pp. 32145–32168, 2023.
- Song, J., Meng, C., and Ermon, S. Denoising diffusion implicit models. In *International Conference on Learning Representations*, 2021.
- Wang, Z., Hunt, J. J., and Zhou, M. Diffusion policies as an expressive policy class for offline reinforcement learning. In *International Conference on Learning Representations*, 2023.

Wu, X., Hao, Y., Sun, K., Chen, Y., Zhu, F., Zhao, R., and Li, H. Human Preference Score v2: A solid benchmark for evaluating human preferences of text-to-image synthesis. *arXiv preprint arXiv:2306.09341*, 2023a.

Wu, X., Sun, K., Zhu, F., Zhao, R., and Li, H. Better aligning text-to-image models with human preference. *arXiv preprint arXiv:2303.14420*, 2023b.

Xu, J., Liu, X., Wu, Y., Tong, Y., Li, Q., Ding, M., Tang, J., and Dong, Y. ImageReward: Learning and evaluating human preferences for text-to-image generation. *Advances in Neural Information Processing Systems*, 2023.

Zhang, C., Vinyals, O., Munos, R., and Bengio, S. A study on overfitting in deep reinforcement learning. *arXiv preprint arXiv:1804.06893*, 2018.

A. Additional Implementation Details

In all experiments, we use Stable Diffusion v1.4 (Rombach et al., 2022) as the base generative model, which ensures consistency with DDPO (Black et al., 2024) and allows for a direct comparison with AlignProp (Prabhudesai et al., 2023), despite their use of v1.5 in AlignProp. In addition, we conduct diffusion model alignment on the LoRA weights (Hu et al., 2022) of the U-Net architecture instead of the full parameter set to reduce memory and computation overheads, following established practices and aligning with official implementations of both DDPO and AlignProp.

DDPO implementations. We use the official PyTorch codebase of DDPO for result reproduction. As discussed in Section 5.2, our TDPO(-R) performs each gradient update in a per-timestep manner with all batch samples averaged, resulting in a higher update frequency (100 gradient updates per epoch) compared to the original DDPO implementation (2 gradient updates per epoch). For a fair comparison, we further reproduce DDPO using the same update frequency (100) and learning rate (1e-4) as ours. Since the PyTorch implementation of DDPO adopts gradient accumulation to reach larger effective batch sizes without requiring additional memory, we adjust its update frequency by reducing the gradient accumulation steps per epoch from $16 \times T$ to 16, where T denotes the number of denoising timesteps with a default value of 50. This leads to two variants of DDPO implementation: DDPO-2 and DDPO-100, differing exclusively in the hyperparameters governing the update frequency and the learning rate. All experiments were conducted on a system equipped with 8 NVIDIA A100 GPUs with 40GB of memory each.

AlignProp implementation. To facilitate a direct comparison, we reproduce AlignProp using Stable Diffusion v1.4, while their reported results are based on v1.5. All experiments were conducted on a system equipped with 4 NVIDIA A100 GPUs with 40GB of memory each, adhering to their default configurations, with an exception of the base model version.

TDPO and TDPO-R implementations. For consistency, the training procedures and configurations of our TDPO are based on the implementation of DDPO-100. Additionally, due to the relatively small parameter size of our temporal critic, we opt for direct training on its entire parameter set. To isolate the effects of our neuron reset strategy, our TDPO-R mirrors TDPO in terms of concurrent components and configurations. All experiments were conducted on a system equipped with 8 NVIDIA A100 GPUs with 40GB of memory each.

Hyperparameter configurations. In Table 1, we list the hyperparameter configurations for all implementations.

Table 1. List of hyperparameter configurations for DDPO-2, DDPO-100, TDPO, and TDPO-R.

Hyperparameters	DDPO-2	DDPO-100	TDPO	TDPO-R
Random seed	42	42	42	42
Denoising timesteps (T)	50	50	50	50
Guidance scale	5.0	5.0	5.0	5.0
Policy learning rate	3e-4	1e-4	1e-4	1e-4
Policy clipping range	1e-4	1e-4	1e-4	1e-4
Maximum gradient norm	1.0	1.0	1.0	1.0
Optimizer	AdamW	AdamW	AdamW	AdamW
Optimizer weight decay	1e-4	1e-4	1e-4	1e-4
Optimizer β_1	0.9	0.9	0.9	0.9
Optimizer β_2	0.999	0.999	0.999	0.999
Optimizer ϵ	1e-8	1e-8	1e-8	1e-8
Samples per epoch	$256 \times T$	$256 \times T$	$256 \times T$	$256 \times T$
Training batch size	8	8	8	8
Training steps per epoch	$32 \times T$	$32 \times T$	$32 \times T$	$32 \times T$
Gradient accumulation steps	$16 \times T$	16	16	16
Gradient updates per epoch	2	$2 \times T$ (100)	$2 \times T$ (100)	$2 \times T$ (100)
Critic learning rate	-	-	1e-4	1e-4
Critic clipping range	-	-	0.2	0.2
Neuron dormant threshold	-	-	-	0
Neuron reset frequency (F / epochs)	-	-	-	10

B. Extended Analyses of Neuron States

The following is an extension of the analyses regarding neuron states discussed in Section 4.2.

Critic dormant neuron percentage. In Section 4.2, we described the effects of resetting different neurons in our critic model on the percentage of dormant neurons. Here we present the experimental results regarding these effects. The left plot in Figure 7 shows the percentage of dormant neurons in our critic model when finetuning on Aesthetic Score. As discussed in Section 4.2, there is a slow ascent of the dormant percentage of neurons in our critic model during training. Resetting dormant neurons consistently reduces the dormant percentage, while resetting active neurons increases it significantly. This further substantiates a conclusion that resetting dormant neurons discourages the presence of dormant neurons, while resetting active neurons discourages the presence of active neurons.

Overlap of dormant neurons. To verify the consistency of dormant neurons in our model, we track the overlap percentage between dormant neurons of nearby steps during the finetuning process. The right plot in Figure 7 shows that the overlap percentage of dormant neurons in our critic model remains a value of 100 through the finetuning process. This indicates that, once a regularization with respect to dormant neurons is learned, then it will continuously affect subsequent training process. Combining this phenomenon with the empirical result we discussed in Section 4.2, which is that resetting dormant neurons in our critic model exacerbates overoptimization, we can further extrapolate that dormant neurons in the critic model act as an adaptive regularization mechanism against overoptimization to imperfect rewards. While resetting dormant neurons may damage this implicit regularization, periodically resetting active neurons offers a potential mitigation strategy, encouraging the model to learn new regularization patterns without forgetting crucial past regularization.

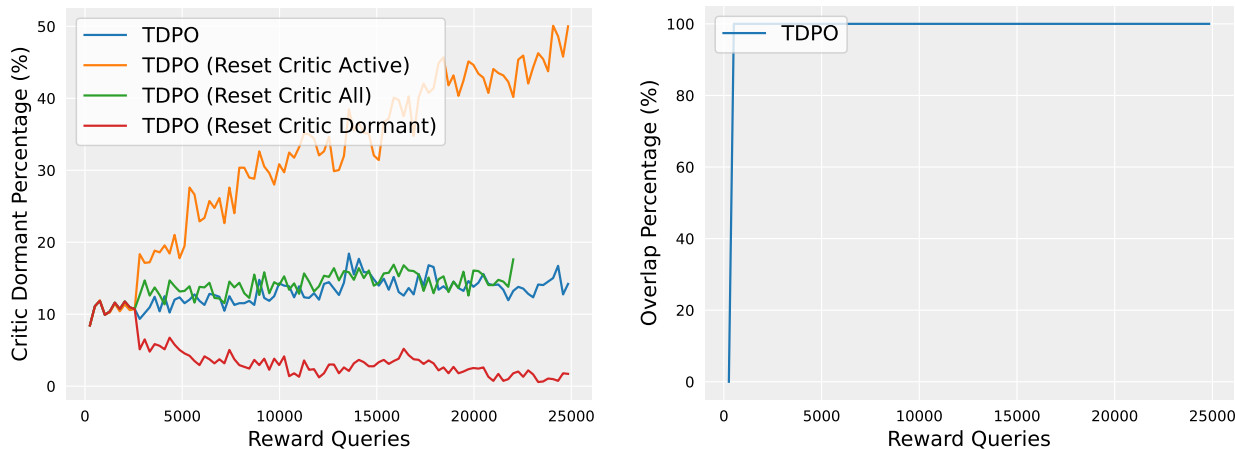


Figure 7. The dormant percentage of neurons (left) and the overlap percentage between dormant neurons of nearby training steps (right) in our critic model when finetuning on Aesthetic Score.

Policy dormant neuron percentage. In Section 4.2, we outlined the observation that a minimal number of dormant neurons is identified within the LoRA layers of our policy model. Accordingly, the left plot in Figure 8 shows the dormant percentage of neurons in the LoRA layers of our policy when finetuning on Aesthetic Score. Notably, the plot indicates that the dormant percentage remains in close proximity to zero throughout the entire training duration when employing a dormant threshold of 0. Consequently, to discern a more pronounced proportion of dormant neurons, we elevated the threshold to 0.1, leading to higher dormant percentages during training. Despite the reduction in dormant neurons following the resets with the threshold of 0.1, discernible effects on cross-reward generalization are not prominently evident, as depicted in Figure 6.

Policy neuron reset. In Section 4.2, we described an effect that resetting active neurons in our policy model causes catastrophic forgetting and heavily hinders learning. Here we present the experimental result regarding this effect. The right plot in Figure 8 shows the effect of periodic resets of policy active neurons on the sample efficiency of TDPO when finetuning on Aesthetic Score. Compared to the original TDPO, the TDPO variant incorporating periodic resets of policy active neurons encounters substantial difficulty in optimizing the reward function, due to the fact that the resets of the overwhelming majority of the model parameters result in the loss of pre-learned knowledge. This unsatisfactory effect can be mitigated by replacing the online-updating scheme with an offline-updating scheme that incorporates a replay buffer to preserve prior knowledge and experiences. We highlight this replacement as an extension of our work for future research.

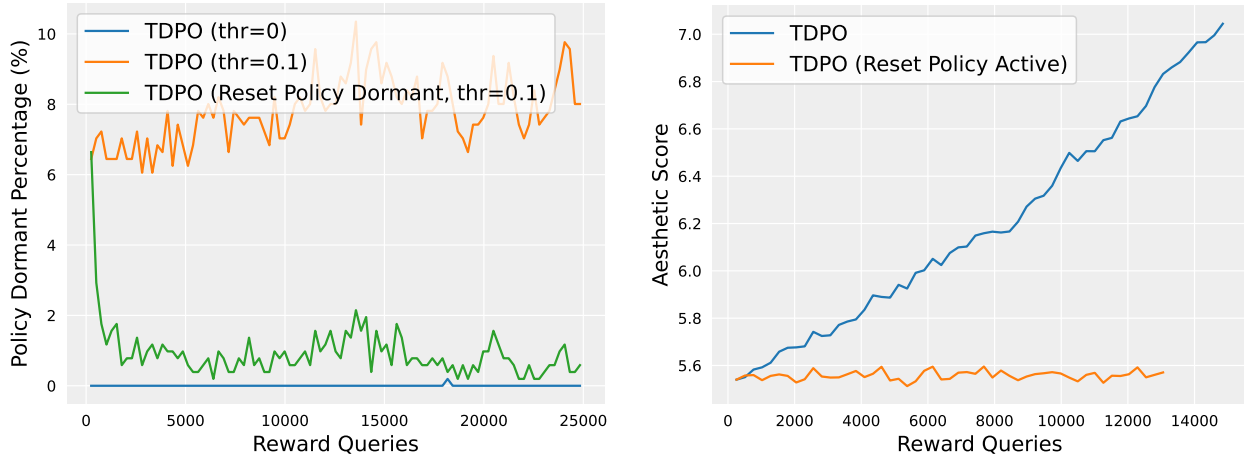


Figure 8. The dormant percentage of neurons in the LoRA layers of our policy (left) and the effect of periodic resets of policy active neurons on the sample efficiency of TDPO (right) when finetuning on Aesthetic Score.

Additional results of cross-reward generalization. Here is an extension of the cross-reward generalization results for different variants of TDPO presented by Figure 6 in Section 5.3. In Figure 9, we show more cross-reward generalization results for TDPO variants with different neuron reset strategies or the KL regularization mechanism. The diffusion models in all variants are finetuned on Aesthetic Score and evaluated on HPSv2 and PickScore. We further investigate the cross-reward generalization capability of TDPO-R by employing an alternative evaluation with leaky ReLU (Maas et al., 2013) instead of the standard ReLU, achieving an even superior performance when evaluating cross-reward generalization against PickScore.

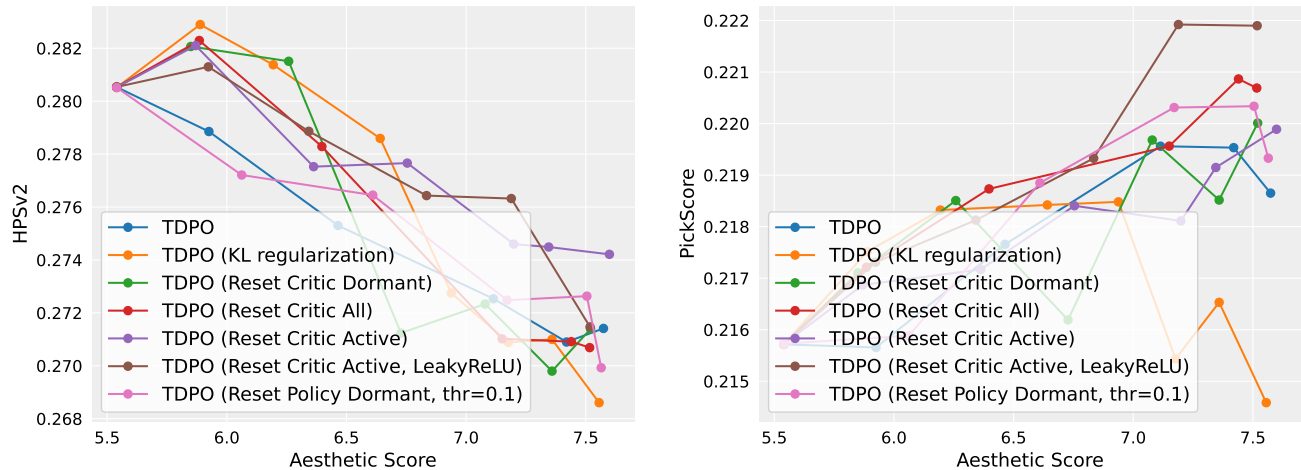


Figure 9. Additional results of cross-reward generalization against HPSv2 (left) and PickScore (right) when finetuning on Aesthetic Score, comparing different variants of TDPO.

C. Generalization to Unseen Prompts

In order to further validate the generalization ability of our methods, here we extend the out-of-domain evaluations of cross-reward generalization to new text prompts that are not previously seen by models during the finetuning process.

Unseen animals. We first employ a novel text prompt set consisting of 8 unseen animal names, including “snail”, “hippopotamus”, “cheetah”, “crocodile”, “lobster”, “octopus”, “elephant”, and “jellyfish”. We conduct evaluations of cross-reward generalization over samples generated using these unseen animal prompts during the finetuning process. In Figure 10, we show the evaluation results when finetuning models on Aesthetic Score via AlignProp, DDPO-2, DDPO-100,

as well as our TDPO and TDPO-R. Notably, our TDPO and TDPO-R still maintain superior performance in cross-reward generalization compared to DDPO and AlignProp. This out-of-domain evaluation demonstrates the robust capabilities of TDPO-R in mitigating reward overoptimization, generalizing effectively to out-of-domain prompts.

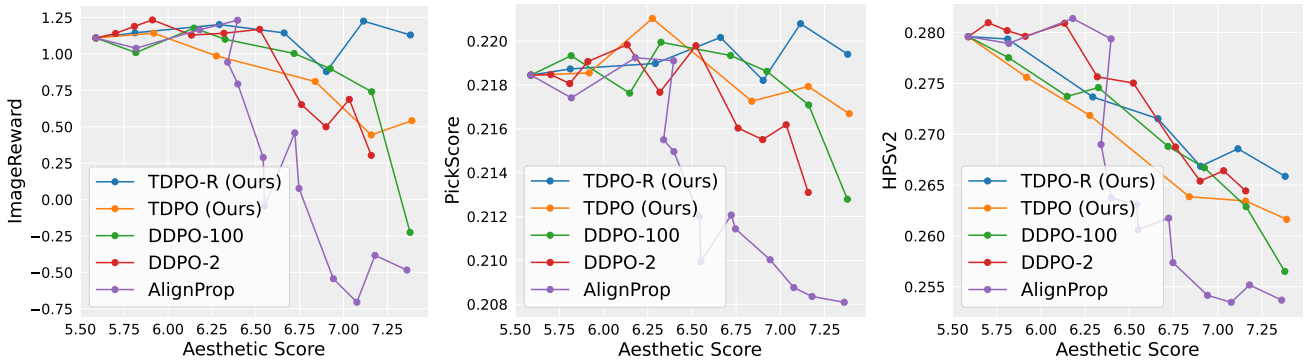


Figure 10. Cross-reward generalization results evaluated on a text prompt set of unseen animals when finetuning on Aesthetic Score.

Color, count, composition, and location. Furthermore, we adopt a set of complex text prompts involving specific color (“A green colored rabbit”), count (“Four wolves in the park”), composition (“A cat and a dog”), and location (“A dog on the moon”) as introduced in (Fan et al., 2023). In (Fan et al., 2023), these prompts are originally used as training text prompts, meaning that they are seen by models during the finetuning process. In contrast, we utilize them as unseen prompts for out-of-domain evaluations while finetuning models on Aesthetic Score, as illustrated in Figure 12. Additionally, Figure 11 shows the image generation results in response to these unseen prompts from models pre-trained or finetuned on Aesthetic Score. Compared to the generation results of other methods, our results are better aligned with the prompts in terms of color, count, composition, and location, and exhibit higher image fidelity, indicating a lower degree of reward overoptimization.

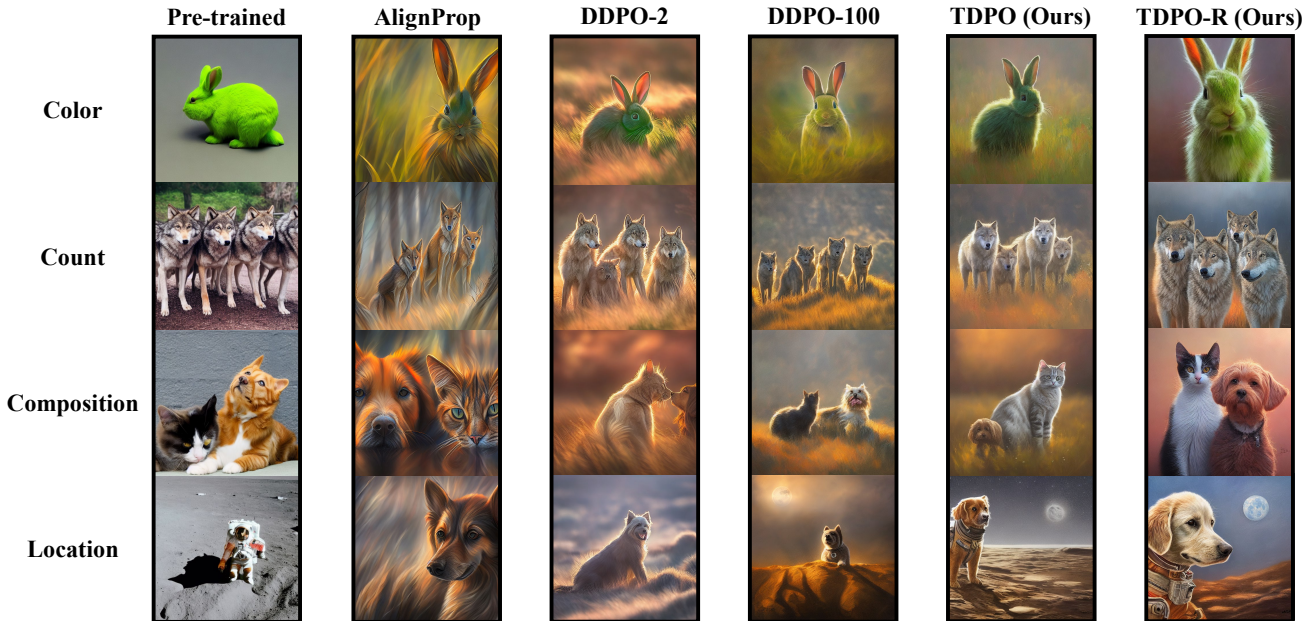


Figure 11. Image generation results of unseen text prompts involving color (“A green colored rabbit”), count (“Four wolves in the park”), composition (“A cat and a dog”), and location (“A dog on the moon”) from models pre-trained or finetuned on Aesthetic Score. For a fair comparison, all images are generated using a fixed random seed of 42, and those from the fine-tuned models achieve the same degree of rewards at around 7 ± 0.1 . Compared to other results, our results are better aligned with the prompts in terms of color, count, composition, and location, and exhibit higher image fidelity, indicating a lower degree of reward overoptimization.

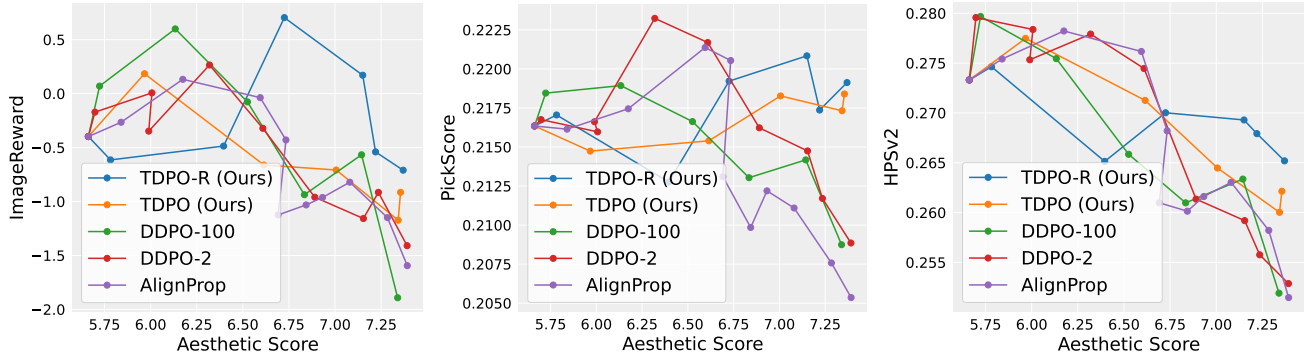


Figure 12. Cross-reward generalization results evaluated over unseen text prompts involving color (“A green colored rabbit”), count (“Four wolves in the park”), composition (“A cat and a dog”), and location (“A dog on the moon”) while finetuning on Aesthetic Score.

D. Additional Qualitative Results

Here is an extension of the qualitative results presented by Figure 5 in Section 5.4. In Figure 13, we present additional qualitative results with high-reward images finetuned on Aesthetic Score. The results from AlignProp and DDPO show notable saturation in terms of style, background, and sunlight, while our generation results manifest greater diversity in these aspects. Specifically, AlignProp generates images characterized by a fixed painting style, while the results from DDPO exhibit a photographic style with similar sunlight angles and similar grassy backgrounds, even in response to prompts like “shark” and “fish”. Conversely, our TDPO and TDPO-R demonstrate the capacity to generate images encompassing both painting and photographic styles, and exhibit an enhanced proficiency in generating diverse and coherent backgrounds aligned with given prompts. In our interpretation, Aesthetic Score characterizes a preference for images that exhibit a stylistic amalgamation, comprising elements reminiscent of both painting and photography. Accordingly, our algorithms ensure effective optimization towards this preference against overfitting a fixed style.

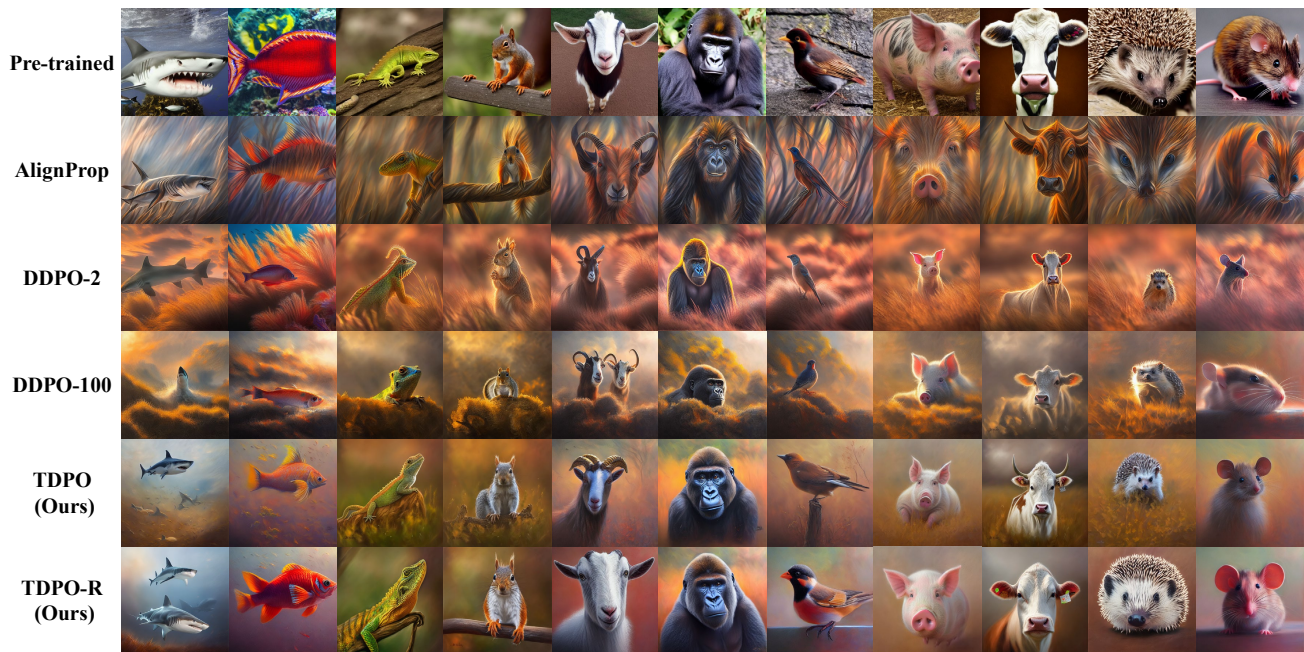


Figure 13. Additional image generation results sampled from models that are exclusively pre-trained or further finetuned on Aesthetic Score via AlignProp, DDPO-2, DDPO-100, as well as our TDPO and TDPO-R. For a fair comparison, all images are generated using a fixed random seed of 42, and those from the fine-tuned models achieve the same degree of rewards at around 7 ± 0.1 .

E. Extended Analysis of Encoder Alignment in Temporal Critic

As introduced in 4.1, the temporal critic leverages the encoder of the target reward model to extract embeddings from each intermediate image of the denoising process. These embeddings serve as the input to a lightweight Multi-Layer Perceptron (MLP) containing only 5 linear layers, with progressively decreasing output dimensionalities of 1024, 128, 64, 16, and 1 unit in the final layer. Crucially, this practice of reusing encoders establishes an alignment between the encoders of both the reward model and the temporal critic. This alignment tends to be critical for overall performance, as it ensures consistency in feature representations and enables the temporal critic to inherit the inductive bias of the reward model during initial training. Beyond performance gains, encoder alignment also offers a compelling advantage in memory efficiency, as the need to store a separate encoder for the temporal critic is eliminated, especially for large pre-trained models like CLIP (Radford et al., 2021) and OpenCLIP-H(Beaumont et al., 2022).

Reward model encoders. Following established practices (Schuhmann et al., 2022; Black et al., 2024), we leverage a pre-trained CLIP model (Radford et al., 2021) as the encoder of the reward model for Aesthetic Score. For the HPSv2 and PickScore reward models, we utilize their official PyTorch implementations, each employing an OpenCLIP-H model (Beaumont et al., 2022) finetuned on human preference data as the encoder. We ensure consistency with these published reward models and their respective rewarding procedures.

Temporal critic encoders. During finetuning on each reward (Aesthetic Score, HPSv2, PickScore), we incorporate the corresponding encoder from the respective reward model into our temporal critic. To delve deeper into the impact of misaligned encoders, we conduct an experiment where the HPSv2 encoder in the temporal critic is replaced with the Aesthetic Score encoder while finetuning on HPSv2. As illustrated in Figure 14, this misalignment lead to a significant decline in TDPO’s reward optimization performance. This finding highlights the critical role of encoder alignment between the reward model and the temporal critic for effective finetuning, as discrepancies in feature representations can hinder the critic’s ability to guide optimization towards the desired reward.

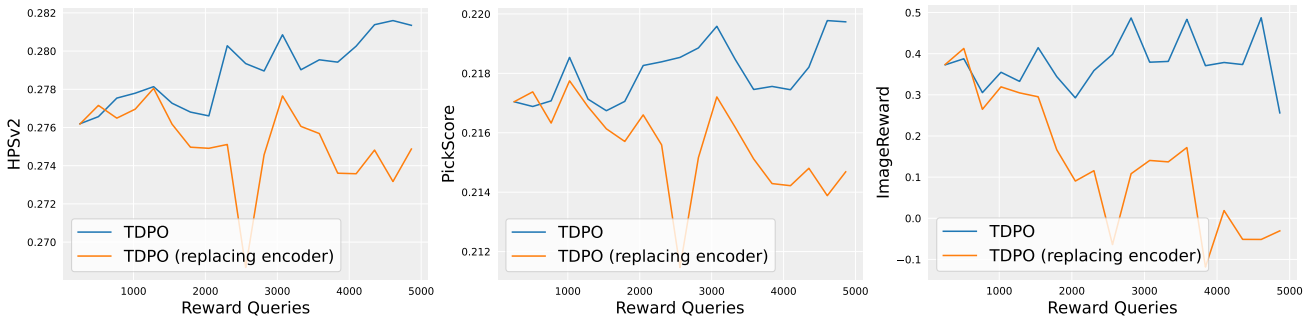


Figure 14. Evaluation results of TDPO’s reward optimization performance when finetuning the diffusion model on HPSv2 and replacing the HPSv2 encoder in the temporal critic with the Aesthetic Score encoder.

F. Extended Related Work

Generation control of diffusion models. Following prior works (Black et al., 2024; Clark et al., 2024) on diffusion model alignment, we incorporate Classifier-Free Guidance (CFG) (Ho & Salimans, 2021) to perform conditional generation of diffusion models. Prior works (Black et al., 2024; Clark et al., 2024) provided compelling evidence that the alignment methods with CFG-based generation control outperform other approaches including prompt engineering and classifier guidance (Dhariwal & Nichol, 2021; Bansal et al., 2023). Accordingly, to maintain clarity and emphasize our improvements in diffusion model alignment, we refrain from conducting comparative analyses on various generation control techniques.

Reinforcement learning for diffusion models. Fan & Lee (2023) first utilize reinforcement learning to train diffusion models. Subsequent studies by Fan et al. (2023) and Black et al. (2024) delve into the utilization of policy gradient-based algorithms to align text-to-image diffusion models with arbitrary reward functions. Instead of finetuning model parameters, Hao et al. (2023) apply reinforcement learning to optimize prompts for text-to-image generation. Beyond the context of text-to-image generation, Wang et al. (2023) undertake the training of diffusion model policies for reinforcement learning, involving backpropagation of a Q-value function through sampling.